ADVANCED MATERIALS INTERFACES

Supporting Information

for *Adv. Mater. Interfaces,* DOI: 10.1002/admi.201900985

Stick-On Large-Strain Sensors for Soft Robots

Sibo Cheng, Yashraj S. Narang, Canhui Yang, Zhigang Suo, and Robert D. Howe**

Supporting Information

Stick-on Large-Strain Sensor for Soft Robots

Sibo Cheng, Yashraj S. Narang, Canhui Yang, Zhigang Suo and Robert D. Howe**

Analytical equations for hydrogel impedance

Following equation (1), we can obtain the theoretical impedance of the hydrogel sensor in a practical circuit. Let a=R_{CT}, $b = 2\pi C_{EDL}$, f be the measuring frequency, and Z_p be the impedance of the equivalent charge transfer resistor and capacitor that comprise the EDL. These quantities satisfy

$$\frac{1}{Z_p} = \frac{1}{Z_{R_{CT}}} + \frac{1}{Z_{C_{EDL}}} = \frac{1}{a} + \frac{1}{\frac{1}{bfj}} = \frac{1}{a} + bfj \tag{5}$$

where j is the imaginary unit. Thus, Z_p is

$$Z_p = \frac{a}{1+abfj} = \frac{a(1-abfj)}{1+a^2b^2f^2} \tag{6}$$

Let $r = R_0$. Then the total impedance of the hydrogel sensor is

$$\begin{aligned} Z_{eq} &= |Z_{total}| = |2Z_p + r| = \left|\frac{2a(1-abfj)}{1-a^2b^2f^2} + r\right| \\ &= \sqrt{(r + \frac{2a}{1+a^2b^2f^2})^2 + (\frac{2a^2bf}{1+a^2b^2f^2})^2} \end{aligned} \tag{7}$$

We use equation (7) to fit the experimental data of the relationship between the equivalent impedance and the measuring frequency in Figure 2c. The best-fit values of the fitting parameters were determined to be $a = 302.93\Omega$, $b = 5.245\times10^{-5}F$ and $r = 893.64\Omega$.

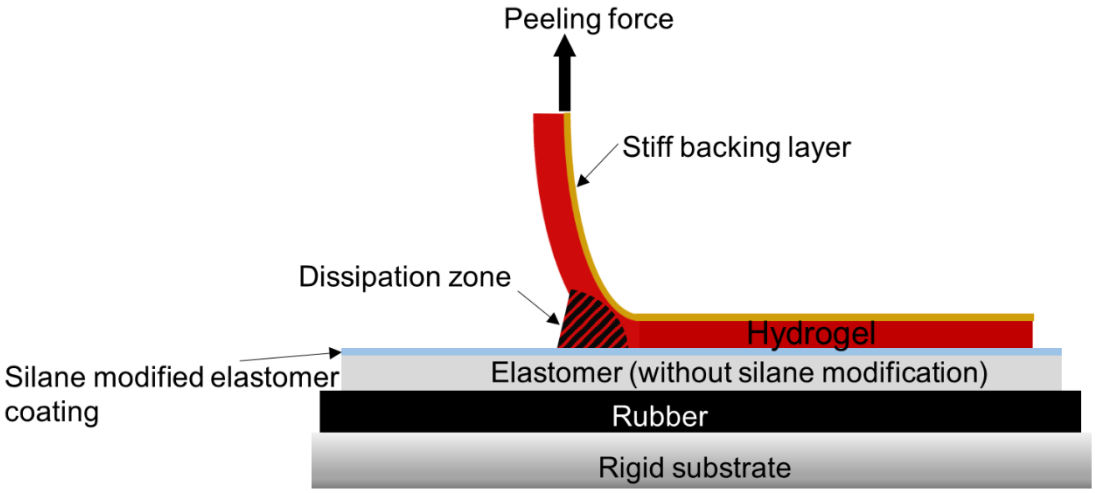

Figure S1. Schematic of the experimental setup for a 90° peeling test to measuring the adhesion between the hydrogel and an elastomer. Because the elastomer cannot be bonded to the rigid substrate (an acrylic sheet) directly, we use another layer of rubber (styrene butadiene rubber) as an interlayer. A stiff backing layer is also bonded to the hydrogel to constrain the stretch of the hydrogel during the test. The peeling speed is fixed at 10 mm·min^{-1}. The hydrogel is TMSPMA-modified PAAm hydrogel containing 8.0 M lithium chloride.

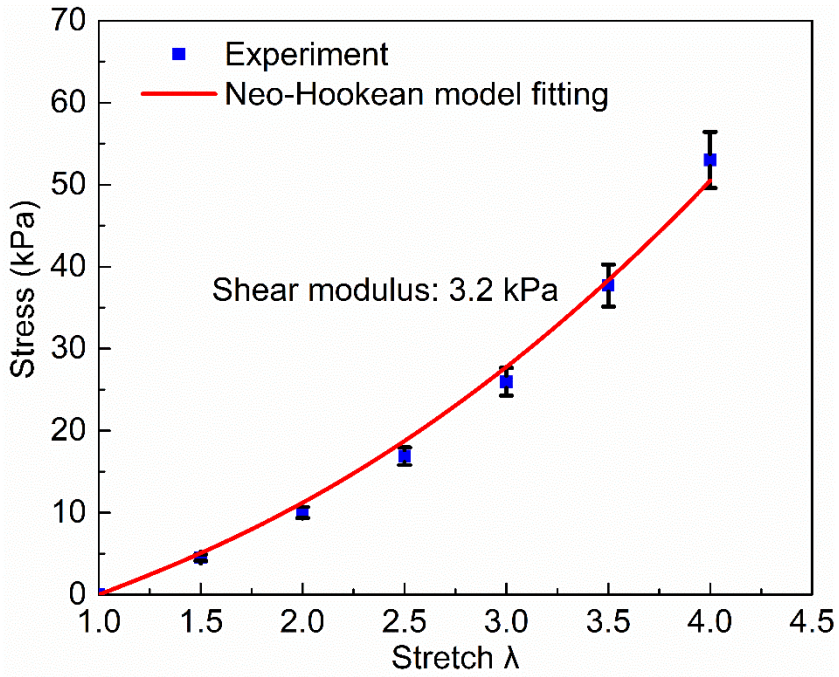

Figure S2. Stress-stretch curve from a uniaxial tensile test of silane-modified PAAm hydrogel containing 8.0 M LiCl. The solid red curve represents the theoretical stress-stretch relationship from a Neo-Hookean model with a best-fit shear modulus of 3.2 kPa.

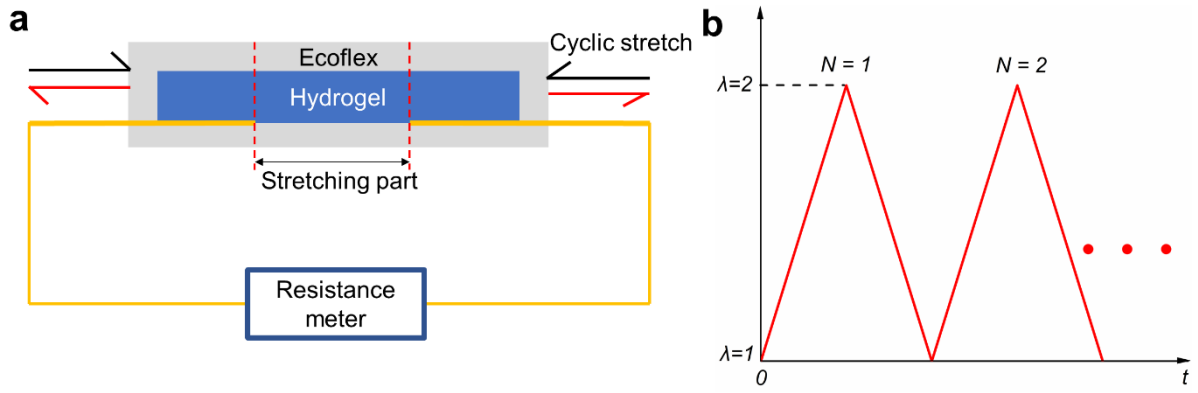

Figure S3. a) Schematic of experimental setup for fatigue testing. A testing sample is sealed by an additional layer of elastomer to maintain stable water content of the hydrogel. The two ends of the hydrogel are connected to a resistance meter. As the sensor is subject to a cyclic stretch, the resistance changes accordingly and is captured by the resistance meter. The measuring frequency is fixed at 10 kHz. b) Loading profile of the cyclic test. The strain rate is 0.066 s^{-1} and the cycle period is 30 s.

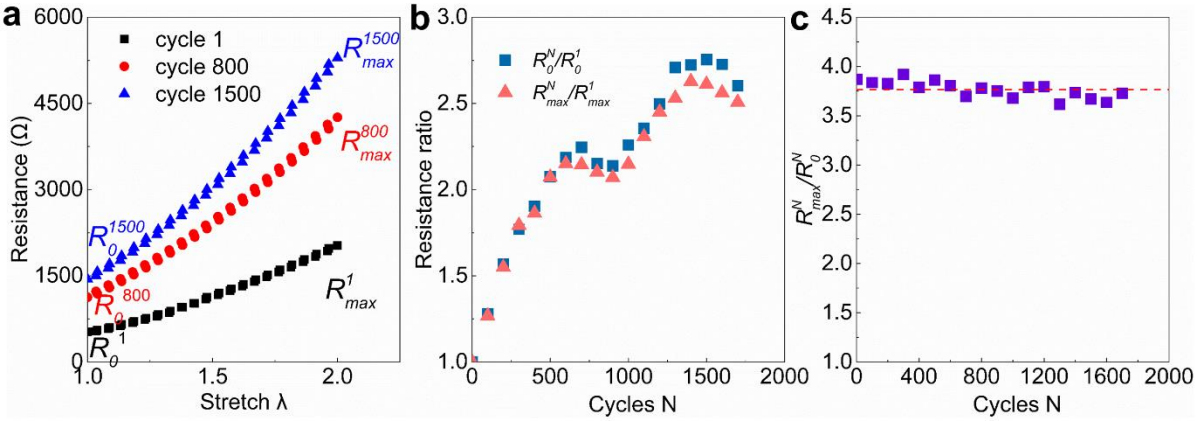

Figure S4. Cyclic stretch of a sensor without an additional layer of elastomer coating. a) Hydrogel resistance changes with stretch. Both R_0 and the maximum resistance R_{max} drift over subsequent cycles. b) The initial and maximum resistance of the hydrogel fluctuates over cycles. As the relative humidity in the environment fluctuates, the hydrogel undergoes swelling due to water gain and de-swelling due to water loss, resulting in fluctuation of the resistance. c) Whereas the resistance of hydrogel keeps fluctuating over time, the ratio of the maximum resistance R_{max} to R_0 at different numbers of cycles remains constant. This result can be explained by the fact that the ratio of R_{max}/R_0 is only related to deformation, but not the absolute value of resistance, as the conductivity of the hydrogel is a material property only depend on water content and ion concentration.

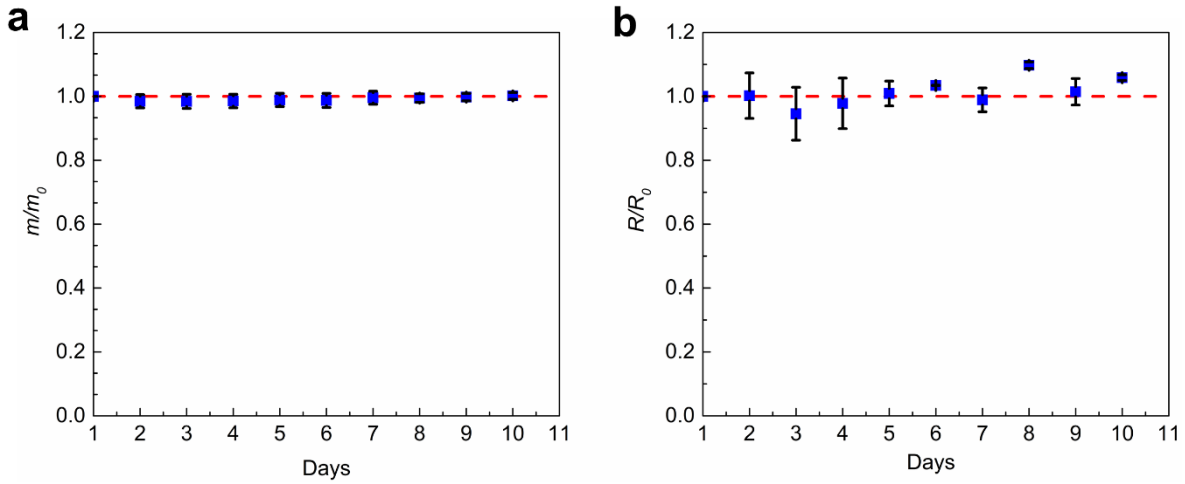

Figure S5. Long-term stability of bare hydrogel sensors. Both a) mass and b) resistance remain stable over ten days. The data represent the mean value and standard deviation of three samples. The samples are stored in open air with a temperature of ~20 ^{o}C and a relative humidity of 20-40%.

Figure S6. 3D-printed mold for casting the pneumatic soft actuator. a) Outer mold of multi-chambered upper section b) Inner mold of multi-chambered upper section c) Mold for strain-limiting base layer.

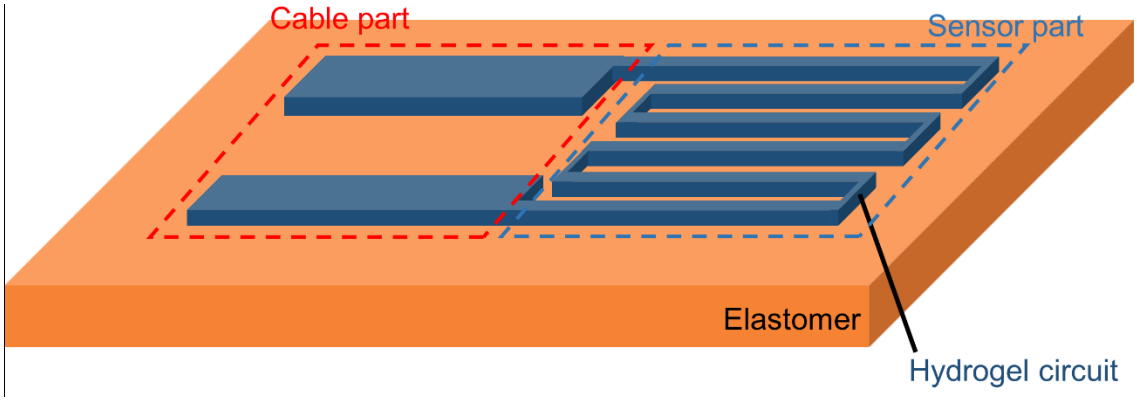

Figure S7. Design of hydrogel circuit for soft robots. For the sensor, the hydrogel is cast into a narrow serpentine pattern to increase the resistance $R_{sensing}$. For the ionic cable, the hydrogel is cast into a straight wide line to decrease the resistance R_{cable}. The ratio of $R_{cable}/R_{sensing}$ is sufficiently small such that during deformation, the resistance change in R_{cable} is negligible compared to the resistance change in $R_{sensing}$.

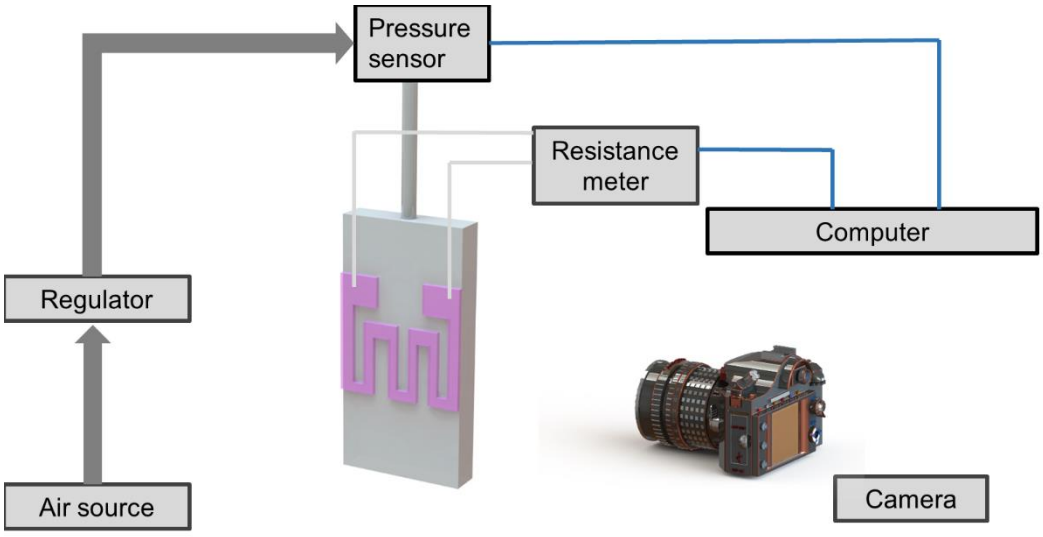

Figure S8. Experimental setup for the characterization of the pneumatic actuator with an integrated hydrogel-based sensor. The air pumped from an air source is fed through a regulator to the pneumatic actuator. The pressure is continuously monitored by a pressure sensor. As the pneumatic actuator is inflated, the hydrogel sensor deforms and changes its resistance accordingly. A resistance meter is connected to the hydrogel sensor to continuously measure the resistance. Both the pressure sensor and the resistance meter are connected to a computer to record the data. A camera is used to photograph the deformation of the actuator, and the images are post-processed to calculate the bending angle.

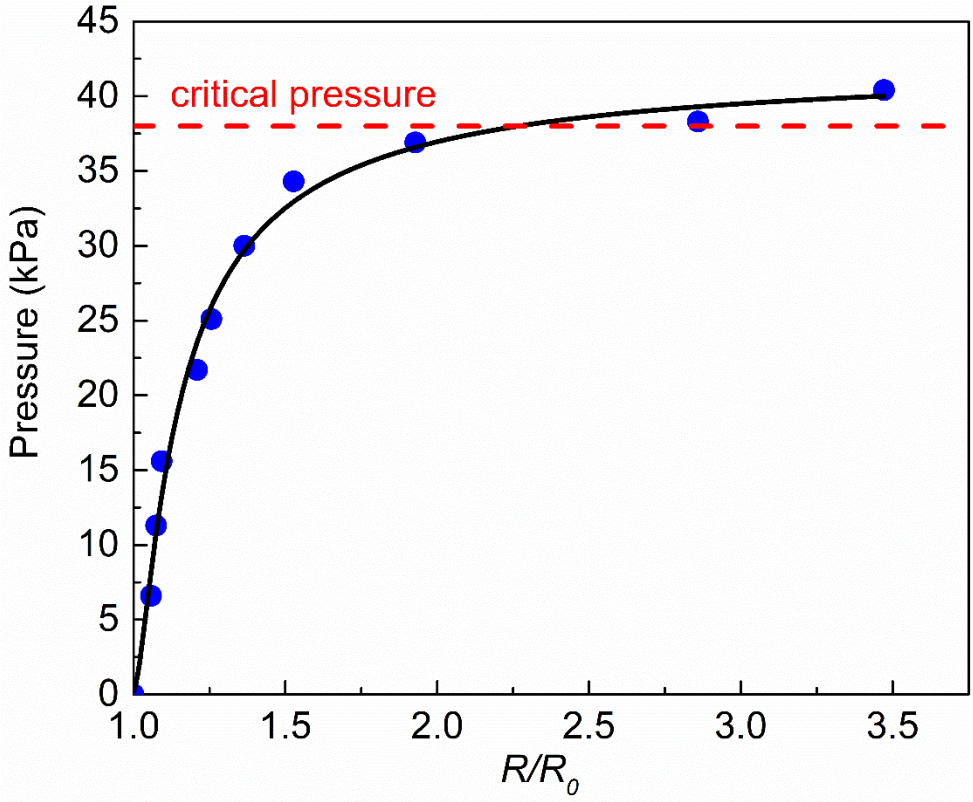

Figure S9. Relationship between pressure in the actuator and the change of resistance of the hydrogel sensor during inflation of the actuator. The actuator shows a significant deformation acceleration when the pressure reaches a threshold (~38 kPa, Supplementary Movie S2). The black line is a guide for the eye.